Color Control in Coaxial Two-Luminophore Nanowires

Alexandre Garreau,[†,*] Florian Massuyeau,[†] Stéphane Cordier,[‡] Yann Molard,[‡] Eric Gautron,[†] Patricia Bertoncini,[†] Eric Faulques,[†] Jany Wery,[†] Bernard Humbert,[†] Alain Bulou,[§] and Jean-Luc Duvail[†,*]

[†]Institut des Matériaux Jean Rouxel, Université de Nantes, CNRS, France, [‡]Institut des Sciences Chimiques de Rennes, Université de Rennes, CNRS, France, and [§]Institut des Molécules et Matériaux du Mans/-PEC, Université du Maine, CNRS, France

ABSTRACT We report a general and simple approach to take control of the color of light-emitting two-luminophore hybrid nanowires (NWs). Our strategy is based on the spatial control at the nanoscale (coaxial geometry) and the spectral selection of the two kinds of luminophores in order to restrict complex charge and energy transfers. Thus, it is possible to control the color of the photoluminescence (PL) as an interpolation of the CIE (Commission Internationale de l'Eclairage) coordinates of each luminophore. For this purpose, we selected a green-emitting semiconducting polymer and a red-emitting hexanuclear metal cluster compound, $(n\text{-}Bu_4N)_2Mo_6Br_8F_6$, dispersed in a poly(methyl-methacrylate) (PMMA) matrix. The great potential and the versatility of this strategy have been demonstrated for two configurations. First, a yellow PL with a continuous change along the nanowire has been evidenced when the proportion of the PPV shell *versus* the nanocomposite core, that is, the green/red volumic ratio, progressively shifts from 1:2 to 1:5. Second, an extremely abrupt change in the PL color with red-green-yellow segments has been achieved. A simple model corroborates the effectiveness of this strategy. PL excitation and time-resolved experiments also confirm that no significant charge and energy transfers are involved. The two-luminophore hybrid nanowires may find widespread nanophotonic applications in multicolor emitting sources, lasers and chemical and biological sensors.

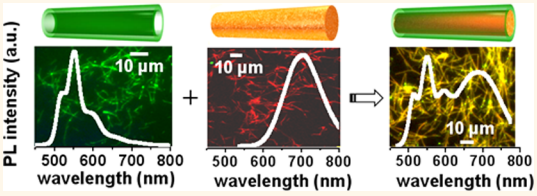

KEYWORDS: hybrid nanomaterial · coaxial nanowire · light-emitting polymer · cluster compounds · luminescence · energy transfer · nanophotonics

Luminescent organic nanowires NWs are of great importance as building blocks in future miniaturized optoelectronic and photonic devices because these systems rely upon the ability to tune the optoelectronic characteristics of the constituent materials. In particular, the potential of organic NWs as nanosources for applications such as tagging,[1,2] sensing,[3−6] lasing,[7,8] display and lighting[9,10] are extensively explored. In each case, the control of emitted light (stability, intensity, color) is a foremost point. For these reasons, many organic nanowires and nanotubes have been fabricated during the last 10 years, either from conjugated polymers,[9,11] or from oligomers or small molecules.[12] Some original emissive behaviors induced by the nanostructuration have also been shown.[13,14] In most cases the organic one-dimensional nanosources are composed of a single luminophore, thus resulting in a single color emission. Then, the color of fluorescence is directly related to the choice of the luminophore among a broad range of dyes or nanoparticles. However, these luminophores have also to meet many other criterions depending on the targeted application, such as the emission quantum yield, the emission stability under illumination or in different media, the solubility, the biocompatibility, *etc*. For this purpose, the study of multiluminophore nanostructures is an emerging and promising domain.[15,16] The mixing of luminophores into nanowires can result in color tuning as well as white emission.[17−21] Moreover, by controlling the position of two luminescent materials at the nanometer scale, it is possible to engineer multicolor nanosources[22] and multisegmented nanowires.[1,2] This strategy is not restricted to pure organic materials but hybrid systems combining both organic and inorganic chromophores (quantum dots, phosphorescent metal complexes) are also of great interest.[20,22−25]

However, the mixing of two or more emissive materials can lead to complex and nondesired behaviors caused by charge and energy transfers between the two luminophores. Reabsorption phenomenon (trivial energy transfer), charge trapping,[26] resonance

* Address correspondence to alexandre.garreau@cnrs-imn.fr, duvail@cnrs-imn.fr.

Received for review July 13, 2012 and accepted March 11, 2013.

Published online March 11, 2013
10.1021/nn400763r

energy transfer (RET) process, *i.e.*, dipole−dipole coupling (Förster energy transfer)[27−29] and electron exchange (Dexter energy transfer)[30] are the main phenomena encountered and they complicate the prediction and the control of the properties.[31] Also, these mechanisms can result in the decrease of the emitted light in a part or in the whole spectral range, thus contributing to the decrease of the overall intensity.[32,33]

The tuning of optical emission by RET mechanisms additionally depends on the pumping wavelength, the absorption, the quantum yield of emitters and the RET efficiency. The RET efficiency depends on the donor-to-acceptor separation distance.[34] Other studies have shown that other parameters are also involved in RET, such as the particle shape and size, the relative spatial distribution of acceptor and donor,[29] the overlapping between the donor absorption spectrum and the acceptor emission spectrum and the relative orientation of the emitters.[21] As a consequence, the design of a new generation of multiluminophore nanoparticles which prevent or restrict complex energy or charge transfer could be suitable to tailor the color of emission.

In this study, we show how a coaxial geometry combining two types of luminophores at the nanometer scale can result in a very fine-tuning of the photoluminescence (PL) features by minimizing the charge and energy transfer mechanisms. Besides the local arrangement of the luminophores, this has been achieved by selecting luminophores which exhibit distinct color of PL emission as well as no significant overlapping of their absorption and emission spectral range. Here, a π-conjugated polymer poly(para-phenylene-vinylene) PPV has been used as a fluorescent green material and metal-clusters compound $(n\text{-}Bu_4N)_2Mo_6Br_8F_6$ as a phosphorescent red one. $(n\text{-}Bu_4N)_2Mo_6Br_8F_6$ is based on $[Mo_6Br_8F_6]^{2-}$ cluster units paired with two ($n\text{-}Bu_4N^+$) counter cations (see Figure S1 in Supporting Information). $(n\text{-}Bu_4N)_2Mo_6Br_8F_6$ is highly soluble and constitutes a useful one-nanometer diameter building block for the elaboration of hybrid nanocomposites[35−37] and functionalization of metal organic framework (MOF).[38] Here, the cluster units were dispersed in an insulating poly(methylmethacrylate) (PMMA) matrix to separate the two luminophores and to avoid charge transfers. The coaxial nanowires with a core of $(n\text{-}Bu_4N)_2[Mo_6Br_8F_6]$@PMMA and a shell of PPV have been successfully synthesized by a template strategy, as demonstrated by electron microscopy. On the basis of a systematic study of micro-PL coupled to micro-Raman investigations along the coaxial NWs, we demonstrate that the resulting PL spectra can be simply decomposed by the sum of the spectrum of each luminophore weighted with their respective proportion. To probe whether transfer mechanisms are involved between the core and the shell, the time-resolved PL emission has been studied for PPV nanotubes, $(n\text{-}Bu_4N)_2[Mo_6Br_8F_6]$@PMMA nanowires and for the coaxial nanowires. This strongly suggests that transfer processes are not significantly involved. Thus, for a given excitation wavelength, it is possible to anticipate and to control the color of the emitted light on the chromaticity diagram as an interpolation of the CIE (Commission Internationale de l'Eclairage) coordinates of each luminophore. Moreover, the original design proposed here also permits to get a very sharp color change within few nanometers, as demonstrated for nanowires with green, red and yellow emitting segments.

RESULTS AND DISCUSSION

Design of Coaxial Two-Luminophore Nanowires. For two or more luminophores based systems, the control of the color is usually achieved by simply mixing organic dyes, quantum dots or other nanoparticles with different ranges of emission. An empirical approach is adopted that consists in changing the proportion of each luminophore. Generally, this strategy promotes complex phenomena occurring when two (or more) kinds of emitters are into contact, that are Dexter and Förster energy transfers as well as charge transfers. To restrain these phenomena, spatial separation of the two kinds of emitters can be achieved by preparing bi- or multilayered thin films. But it does not circumvent the self-absorption phenomenon due to overlapping of the absorption and emission spectra. The original design proposed here enables us to address these points and finally to anticipate the emitting color along nanowires with a control at the nanoscale. This control has been demonstrated here with individual nanowires exhibiting either a uniform yellow color, a progressive change from yellow to orange, or a sharp shift of the color from yellow to green and red segments (Figure 1).

First, we selected the PPV conjugated polymer as a green emitter and $(n\text{-}Bu_4N)_2[Mo_6Br_8F_6]$ cluster compound as a red emitter because the absorption band of the cluster unit (red dashed line, peak at ∼3.8 eV) has no significant overlap with the emission band of the PPV (green line, peak at ∼2.2 eV) as shown on Figure 1a. Thus, the absorption by the cluster units of the photons emitted by PPV cannot significantly occur. Figure 1b shows epi-fluorescence micrographs of random PPV nanotubes and $(n\text{-}Bu_4N)_2[Mo_6Br_8F_6]$@PMMA composite nanowires mats synthesized as reference systems. Uniform bright green and red characteristic of PPV and $(n\text{-}Bu_4N)_2[Mo_6Br_8F_6]$ emissions are observed.

Aside from the necessary spectral separation, the spatial separation is also required. Indeed, Dexter energy transfer occurs when the wave functions of the two types of luminophores overlap. This implies that the excited donor and the ground-state acceptor are close enough (typically ∼0.6−2 nm). For charge transfer phenomenon, a similar distance between the donor and the acceptor is needed. Concerning Förster energy transfer, the process is efficient for typical distances 5−10 nm between the

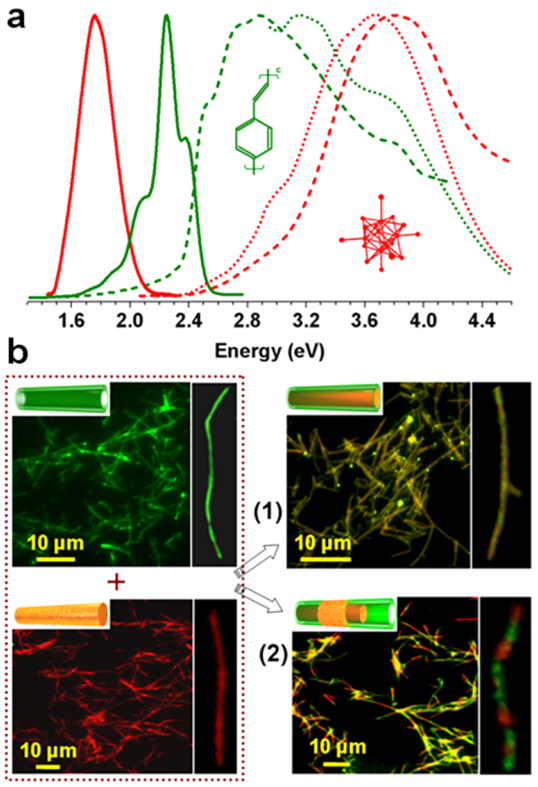

Figure 1. (a) Normalized absorption (dashed lines), excitation (dotted line, λ_{em} = 710 and 500 nm for $(n\text{-Bu}_4\text{N})_2[\text{Mo}_6\text{Br}_8\text{F}_6]$ cluster compound and PPV, respectively) and photoluminescence (solid lines, λ_{exc} = 400 nm) spectra of the $(n\text{-Bu}_4\text{N})_2[\text{Mo}_6\text{Br}_8\text{F}_6]$ cluster compound (red lines) and of the PPV polymer (green lines). These spectra are measured for spin-coated thin films. The cluster and polymer structures are shown as insets. (b) Fluorescence microscopy images (λ_{exc} = 330−380 nm; λ_{em} > 420 nm) of dispersed PPV nanotubes (green), $(n\text{-Bu}_4\text{N})_2[\text{Mo}_6\text{Br}_8\text{F}_6]$@PMMA nanowires (red) and coaxial nanowires for the two coaxial arrangements: (1) continuous PPV shell (yellow NWs) and (2) discontinuous PPV shell (red-green-yellow segments): schematic illustration of $(n\text{-Bu}_4\text{N})_2[\text{Mo}_6\text{Br}_8\text{F}_6]$@PMMA composite NWs, PPV NTs and coaxial NWs are given in insets. A magnified view of a single nanowire is shown on the right side of each image.

donor and the acceptor.[29] In our system, the spatial separation was achieved by dispersing the cluster units in an insulating PMMA matrix to form a hybrid composite $(n\text{-Bu}_4\text{N})_2[\text{Mo}_6\text{Br}_8\text{F}_6]$@PMMA and by using a secondary template strategy. First, a thin layer of PPV was deposited by impregnation of porous alumina membranes. Then, a solution containing both the PMMA and the cluster units was used to fill PPV nanotubes. This results in a coaxial arrangement where the two luminophores are spatially well-separated at the nanoscale with a composite $(n\text{-Bu}_4\text{N})_2[\text{Mo}_6\text{Br}_8\text{F}_6]$@PMMA core and a PPV shell as illustrated in Figure 1b (see the Methods part for further details).

Coaxial Nanowires Characterization. The coaxial NWs were characterized using a scanning electron microscope (SEM), an atomic force microscope (AFM) in intermittent contact mode and a transmission electron microscope (TEM) equipped with an energy dispersive X-ray spectrometer (EDX) after removing the alumina template. A mat of flexible NWs (Figure 2a) is obtained, confirming that the procedure successfully generated NWs at high yield ($\sim 10^9$ per template), as well as dispersed individual NWs (insets of Figure 2a,b). Their lengths were found in the range 10−20 μm while the membrane thickness is about 60 μm. This difference can be explained by the alumina removal step and the sonication step required for their dispersion in solution, which result in shortening of the NWs.

The contrast provided by the heavy atom of molybdenum ($Z = 42$) from the cluster units, present in the core, compared to mainly carbon in the shell allows to clearly distinguish the coaxial morphology of NWs by TEM analysis (Figure 2c). Statistical analysis of micrographs yielded average values for NWs outer diameter, $\sim$200−250 nm, and the shell thickness of about 20 nm, in agreement with TEM studies of the shell of PPV nanotubes published previously.[39] The disparity of NWs diameters reflected the inhomogeneous internal pore diameters within the template employed. The coaxial geometry is unambiguously demonstrated by the EDX study. Figure 2d shows two EDX spectra performed with 10 nm diameter spot size measured for the NWs core (blue circles) and the NWs shell (red circles) in Figure 2c. It is clear from the peaks corresponding to molybdenum and bromine that the $[\text{Mo}_6\text{Br}_8\text{F}_6]^{2-}$ cluster units are only located within the core of the NW, while the carbon dominates for the PPV shell. The presence of phosphorus and copper results from the removal of the template by phosphoric acid and from the TEM grid, respectively. The EDX peak at 1.5 keV cannot be clearly attributed to bromine or aluminum and arises probably from a mixture of the two contributions. The lack of contrast within the core part strongly suggests that the cluster units are homogenously dispersed into the PMMA matrix. This is in agreement with selective area electron diffraction (SAED) study, not shown here. The absence of diffraction features in SAED pattern indicates that there is no crystallization of the cluster compounds. The $(n\text{-Bu}_4\text{N})_2[\text{Mo}_6\text{Br}_8\text{F}_6]$@PMMA composite can thus be considered as homogeneous, a foremost point for the targeted control of the color all along the nanowire. Indeed, more concentrated areas of cluster units would result into a locally more intense red emission and thus into inhomogeneous color along the NW due to a local change in the balance between the red and the green emission.

The successive impregnation of the template by the PPV and the composite simply produces the coaxial geometry of nanowires. To demonstrate the versatility to change the emission color permitted by this coaxial arrangement, two designs have been processed, as shown in Figure 1: (1) a continuous PPV shell, it results in a uniform bright yellow-orange emission along the NWs; (2) a discontinuous PPV shell results in multisegmented NWs with red, green or yellow segments.

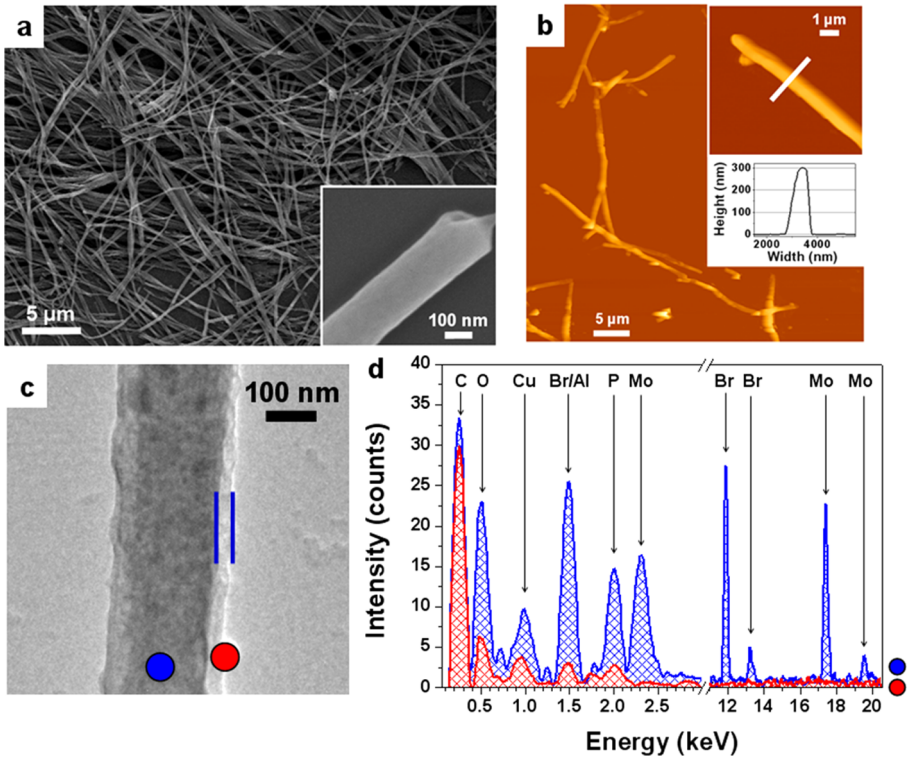

Figure 2. (a) SEM image of a mat of flexible coaxial NWs. Inset: magnified SEM image of an isolated NW. (b) AFM height image of a network of wires deposited onto a glass substrate (*Z*-scale: 1 μm). Inset: magnified AFM height image of a NW with topography line profile measured across the wire at the indicated location. (c) TEM micrograph of an isolated NW which reveals the coaxial geometry, *i.e.*, a PPV shell (indicated by the blues lines) and a $(n\text{-}Bu_4N)_2[Mo_6Br_8F_6]$@PMMA composite core as confirmed by EDX measurements (d) at the locations indicated on panel c (the circles represent roughly the probe area). Red and blue spectra correspond to the shell and the core of the fiber, respectively.

The relation between the proportions of each material and the color along the NWs has been established by micro-Raman and microphotoluminescence spectroscopy studies, as reported below.

Spectroscopic Studies along the Nanowires. To evaluate the proportions of each material along the NWs and the corresponding emitted color in the case of a continuous PPV shell, the anodic alumina oxide (AAO) templated NWs were revealed by making a cross section as illustrated in Figure 3. This cross section was then scanned by a focused laser and micro-Raman (Figure 3a) and micro-PL (Figure 3c) spectra were recorded at different positions from top to bottom of the membrane. The spot size of the focused laser beam on the sample was estimated to be about 1−2 μm. For the Raman study, a spectrum was recorded every 6 μm for the 60-μm long NWs. The Raman peaks below 300 cm^{-1} were attributed to the hexanuclear molybdenum cluster,[40−42] whereas peaks at 814, 882, 930, and 1453 cm^{-1} were attributed to PMMA.[43−45] The Raman characteristic peaks at 1174, 1550, 1588, and 1631 cm^{-1} correspond to the stretching and the bending modes of carbon bonds in the PPV molecular backbone.[46] The presence of the peaks related to the PPV, PMMA and clusters corroborates the successful synthesis of coaxial NWs, as shown by TEM. Most importantly, the variation of the corresponding Raman peak intensity along the scanning direction is a direct signature of the quantity of each material. This effect has been exploited to evaluate the variation of the proportion of each material along the 60-μm long NWs. Indeed, the choice of the membrane and the wetting conditions can directly affect the quantity of matter deposited inside the nanopores. We have shown recently that PPV NWs can be prepared in polycarbonate membranes while PPV NTs are generally formed into AAO membranes.[47] Here, the evolution of the proportion of PPV and clusters compounds has been determined from the change in the Raman intensity for 10 spectra (Figure 3b). After a strong decrease of the Raman signal for both PPV and clusters from the impregnation side, the intensity (normalized to the value at the first, *i.e.*, top position) stabilizes around 0.5−0.6 for the cluster units while the PPV one keeps falling down to 0.2 when probing down to the opposite side of the membrane cross-section. Such a decrease of the intensity can directly be attributed to less matter deposited. Indeed, it is expected for a solvent-assisted wetting synthesis that the quantity of polymer in solution decreases when it further penetrates from the top impregnation side to the bottom of the pores. This results in a thinner nanotube wall, also corroborated by TEM investigation. Considering a NW diameter of 200 nm, the thickness of the PPV shell can vary from

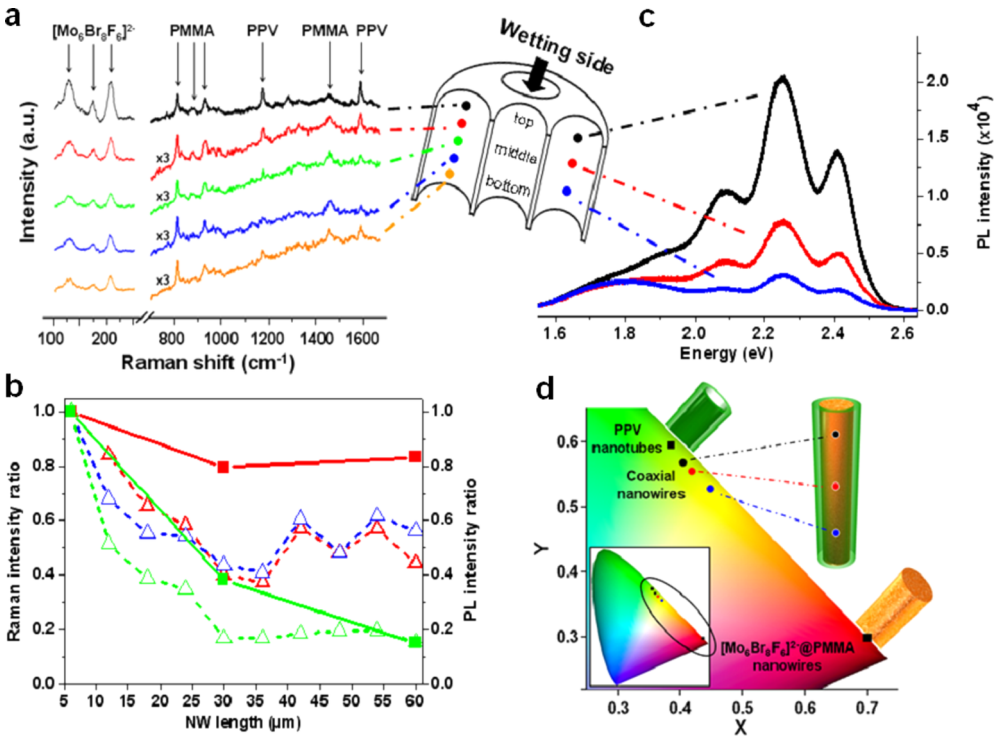

Figure 3. (a) Micro-Raman spectra of array of coaxial NWs embedded in Al_2O_3 matrix for five laser positions (λ_{exc} = 785 nm) along the pores as illustrated in the scheme. The assignment of characteristic Raman peaks is also reported. (b) Micro-Raman intensity (dashed lines) of PMMA (814 cm^{-1}, blue), (n-Bu_4N)$_2$[$Mo_6Br_8F_6$] (206 cm^{-1}, red) and PPV (1550 cm^{-1}, green) *versus* the cross-sectional position in the membrane reported from Figure 3a. Right axis: PL intensity (solid lines) *versus* the position for the 2.25 eV (green) and the 1.77 eV (red) bands related to PPV and clusters compounds, respectively. (c) Micro-PL spectra (λ_{exc} = 457.9 nm) of coaxial NWs for the three positions top-middle-bottom along the pores as illustrated in scheme. The correspondence between the micro-PL spectra and the perception color is represented in a chromaticity diagram (d). CIE coordinates for pure PPV nanotubes and (n-Bu_4N)$_2$[$Mo_6Br_8F_6$]@PMMA NWs are also reported.

about 20 nm (top) to 10 nm (bottom). Then, the corresponding volumic ratios of green (PPV) *versus* red ((n-Bu_4N)$_2$[$Mo_6Br_8F_6$]@PMMA) emitters have been estimated to vary approximately from 1:2 (shell thickness of 20 nm) to 1:5 (shell thickness of 10 nm) along the nanowires. We emphasize that the respective proportions of the two emitters are very similar in our coaxial approach. Thus, it is possible to tune the color of emission either in a slight way as shown here, or very sharply (see Figure 1) only by changing the thickness of the shell. Additionally, we propose two methods to increase the tuning range. First, a larger change in the shell thickness along the coaxial nanowire may result in a broader change of the covered color range: the sharper the variation of shell thickness, the stronger the shift of color. Second, an increase in the cluster concentration within PMMA may result in a larger weight of the red spectrum in the overall spectrum, *i.e.*, a global red shift of the color range. A similar effect is expected for other couples of luminophores, while respecting the spectral restrictions reported above. This dramatically contrasts with the common strategy used for tuning the color that consists in the direct mixing of the two (or more) emitters with typical donor–acceptor molar ratios of 100:1.[18] Such a discrepancy between the two kinds of luminophores can be a drawback for in-solution processes, because the limit of solubility of the two emitters may constrain the donor–acceptor ratio, *i.e.*, the resulting color. Based on this variation in the proportion of the two luminophores and considering the quantum yield equals to about 40% for the PPV when processed into nanotubes[47] and about 20% for the (n-Bu_4N)$_2$[$Mo_6Br_8F_6$],[48,49] a progressive shift of the color can indeed be anticipated from yellow-green to yellow-orange from top to bottom of the NWs.

The emissive features of the as-prepared NWs have been investigated by steady-state PL with a 2 μm diameter microprobe at three positions along the membrane pores, as show in Figure 3c. The wide spectra are composed of the characteristic PPV PL bands centered at 2.40, 2.24, 2.07, and 1.88 eV and of the cluster broad band with a maximum at 1.77 eV. It is clear from Figure 3c that the PL contribution of PPV is strongly reduced from top to the bottom of the cross section with respect to the nanocomposite signal. The change in the PL intensity for the 2.24 and the 1.77 eV bands is reported on the right axis of Figure 3b. The PL decrease appears to be well-correlated to the Raman intensity decrease. A more detailed analysis with a simple model to fit the PL spectra is given later.

Color Control and Spectral Modeling. The effect of the monochromatic pumping wavelength on the emission

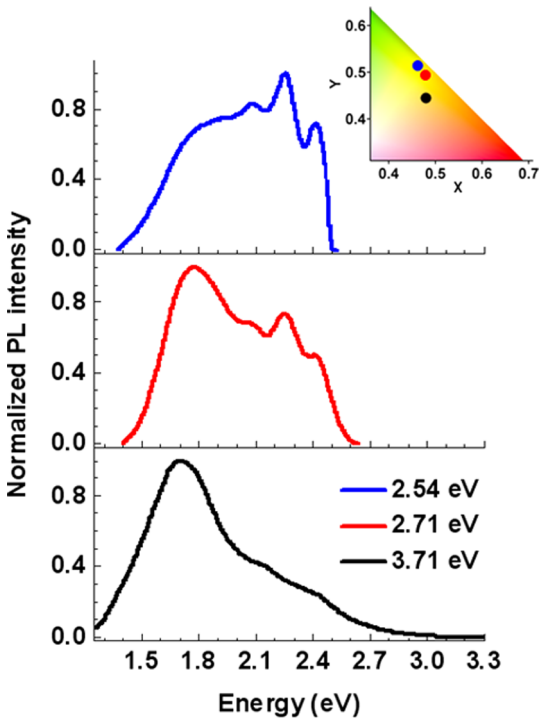

Figure 4. Effect of the energy of excitation (2.54, 2.71, and 3.71 eV) on the PL spectrum of the coaxial nanowires and their respective color on a chromaticity diagram (inset). The investigated area along the NWs (in AAO template) is the same for the three spectra.

color was first determined. Considering that the PPV and the clusters units have different absorption spectra (Figure 1), the monochromatic pumping can favor resonant pumping of one species. Here, the PL spectra reported on Figure 4 were measured under a microprobe at the same position along the nanowires and for pumping at 3.71 eV (334 nm), 2.71 eV (458 nm), and 2.54 eV (488 nm). It is clear that the contribution of the PPV spectrum progressively increases with respect to the $(n\text{-}Bu_4N)_2[Mo_6Br_8F_6]$@PMMA one when the excitation line shifts from 3.71 to 2.71 and to 2.54 eV. Such a variation can be anticipated from the absorption, emission and excitation spectra on Figure 1 (see also photoluminescence excitation maps in Supporting Information), due to the preferential resonance pumping with the clusters for an excitation line in the UV range and with the PPV for excitation in the visible blue range. It can also be noted a broadening of the overall spectrum for the excitation at 3.71 eV, which is due to the superimposed broadened emissions of the two chromophores at this excitation energy. In addition, the sharp drop in the PL intensity at 2.50 eV for an excitation at 2.54 eV is due to the edge filter used to eliminate the Rayleigh contribution. For these reasons, the points reported in the chromaticity diagram are not aligned (inset of Figure 4). In the following, the color was investigated for a fixed pumping wavelength.

We now address the color control. For this purpose, the coaxial NWs with a continuous PPV shell are considered

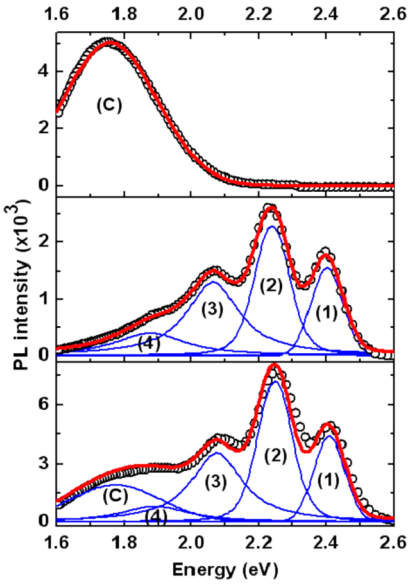

Figure 5. Emission spectrum (black circle) of $(n\text{-}Bu_4N)_2[Mo_6Br_8F_6]$@PMMA NWs (upper graph), PPV nanotubes (middle graph), and coaxial NWs (lower graph) embedded in the Al_2O_3 membrane at the middle position, as shown in Figure 3. These spectra were fitted with Voigt functions (blue solid lines). The cumulative fits with the model proposed are plotted in red.

(see Figure 1b, case 1). The color emission corresponding to each PL spectrum (pumping wavelength: 2.71 eV) has been determined for three positions along the NWs and reported in a chromaticity diagram (Figure 3d: top, $x = 0.41$, $y = 0.57$; middle, $x = 0.42$, $y = 0.55$; bottom, $x = 0.45$, $y = 0.53$). The coordinates of $(n\text{-}Bu_4N)_2[Mo_6Br_8F_6]$@PMMA NWs ($x = 0.70$, $y = 0.30$) and PPV nanotubes ($x = 0.38$, $y = 0.60$) are also reported. It can be noted that the perception of the emission color for the coaxial NWs is closer to the PPV one, due mainly to the sensitivity of the human eye. Moreover, the contribution of the PPV emission is favored by the higher quantum yield of PPV and the pumping wavelength (2.71 eV), as discussed above. As anticipated from the Raman study, the reduced quantity of PPV from top (impregnation side) to bottom of the NWs results in a progressive shift of the color from yellow-green to yellow-orange. It is emphasized that the coaxial design is a versatile strategy which makes possible to have either a slight color shift for a progressive change of the shell thickness, or a very sharp color change for a discontinuous shell.

Next, we show that complex behaviors caused by charge and energy transfers between the two luminophores are not significantly involved in the hybrid coaxial NWs. As discussed above, the spectral features of the selected two luminophores and the original design with the coaxial geometry and the insulating matrix for the cluster units are expected to prevent from reabsorption phenomenon, charge trapping, resonance energy transfer process and electron exchange. If they occur, such phenomena would result in the decrease of the donor (green) emission intensity,

and the increase in the acceptor (red) emission intensity when compared to the case without transfer. This is obviously not the case as a dominant bright yellow emission is obtained for a volumic green (PPV):red (PMMA-cluster) ratio equal to 1:2 to 1:5 in the NWs with a continuous shell. This qualitative observation is confirmed by the following quantitative analysis. Considering that for the coaxial NWs, any coupling between the two luminophores would involve changes in the spectral shape with respect to the single luminophore case, a simple model has been tentatively implemented. It is proposed that the spectrum for the coaxial nanowires results from the sum of the PPV and cluster spectra weighted with only two parameters P_{PPV} and $P_{Cluster}$ related to the proportion of each luminophore:

$$[\text{Coaxial spectrum}] = P_{PPV}*[\text{PPV spectrum}] + P_{Cluster}*[\text{Cluster spectrum}]$$

In this model, for the three positions along the cross section (top, middle and bottom, see Figure 3), the spectrum of the PPV nanotubes was fitted with four Voigt functions (noted (1), (2), (3) and (4)) corresponding to the four bands usually identified for PPV,[50] while the spectrum for $(n\text{-}Bu_4N)_2[Mo_6Br_8F_6]$@PMMA composite NWs was fitted with a Voigt function noted (C) (a complete description of the fitting method is reported in Supporting Information). The corresponding curves are reported in Figure 5 for the spectra measured in the middle of the membrane cross sections (see Supporting Information for the fits of the spectra at the top and bottom positions and for details of the fitting parameters). Then, the spectra for the coaxial two-luminophore nanowires were tentatively fitted by the sum of the PPV and cluster contributions with fixed values for the energy of the emission bands and the width parameters. Only the magnitudes with respect to PPV and composite spectra were allowed to vary freely, corresponding to the proportion of each material as described in the model. Finally, the band widths were allowed to slightly vary. A very good fit was obtained for the top, the middle and the bottom spectra, as shown in Figure 5 and Supporting Information. To further corroborate the validity of our analysis, the fitting components areas (related to the width and the magnitude) for the four PPV bands and the cluster one in two-luminophore NWs were compared to the corresponding values for the one-luminophore NWs or NTs (Figure S4 and Table S3 in Supporting Information). Remarkably, for each position (top, middle, and bottom), the areas for one-luminophore or two-luminophore systems are very similar. Moreover, their intensity exhibits a variation with the position along the NW close to the one observed for the Raman intensity. This analysis shows that for our system, the very simple model with only two free parameters P_{PPV} and $P_{Cluster}$ related to the proportion of each luminophore is well verified.

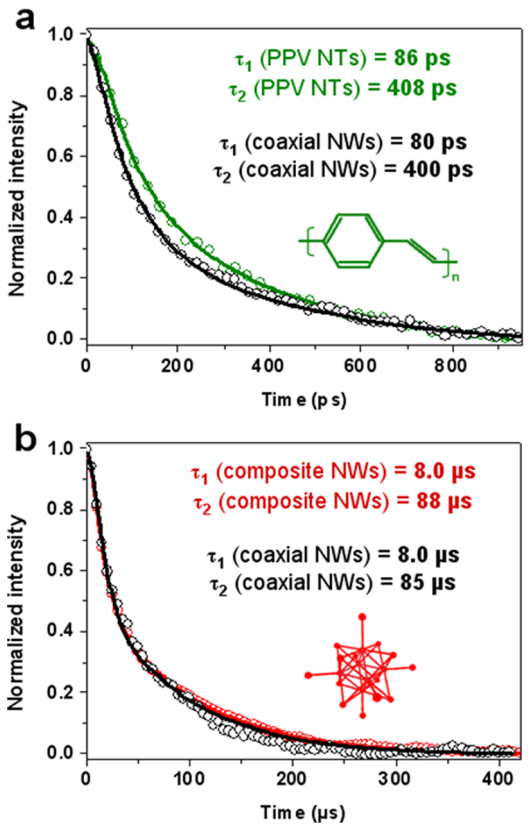

Figure 6. Photoluminescence decay curves and calculated decay times of (a) PPV nanotubes (green curves) and coaxial composite(core)-PPV(shell) NWs (black curves) integrated in the 510−570 nm spectral range, and (b) composite $(n\text{-}Bu_4N)_2[Mo_6Br_8F_6]$@PMMA NWs (red curves) and coaxial NWs (black curves) integrated in the 670−730 nm range. In each case, circles and solid lines correspond to experimental points and fitted curves, respectively.

Furthermore, the energy transfer dynamics was investigated by time resolving the PPV and $(n\text{-}Bu_4N)_2[Mo_6Br_8F_6]$ optical emission upon excitation at 3.10 eV (400 nm). The direct comparison between the decay of a given luminophore in pure NWs or in hybrid coaxial NWs is expected to evidence any transfer mechanism between PPV and cluster units. Figure 6a shows fluorescence decay curves of the PPV NTs and the coaxial NWs integrated in the 510−570 nm emission range and during 1 ns, whereas Figure 6b shows phosphorescence decay curves of the $(n\text{-}Bu_4N)_2[Mo_6Br_8F_6]$@PMMA NWs (red) and the coaxial NWs (black) integrated in the 670−730 nm emission range and during 1 μs. These experimental decays were fitted with a biexponential function and the corresponding decay times are mentioned in the inset of Figure 6. In both cases (Figures 6a,b), the luminescence decay times measured in the hybrid coaxial NWs are very close to the values measured for the NWs or NTs made of a single type of luminophore. This is strong evidence that there is no significant charge and energy transfer between $(n\text{-}Bu_4N)_2[Mo_6Br_8F_6]$@PMMA and PPV polymer in the coaxial NWs. A discussion of the possible

effects of the coaxial morphology on energy transfers in our system is now proposed. For the PPV, the exciton diffusion length is typically 5−12 nm.[51,52] Thus, for a PPV shell thickness of about 20 nm, almost all the excitons created in PPV could diffuse toward the interface and thus eventually interact with clusters units embedded in PMMA. A fluorescence resonance energy transfer (FRET) mechanism between the two luminophores should then strongly affect the contribution of PPV to the overall PL spectrum and PL decay. From the stationary and time-resolved PL studies and analysis, it is reasonable to consider that no significant energy transfer takes place in our system. Additionally, the proportion of clusters located in the dipole−dipole like coupling area close to PPV can be estimated. Indeed, the FRET efficiency is inversely proportional to the sixth power of the distance between the donor and acceptor.[53] Previous studies in composites with quantum dots suggested nonradiative resonant dipole−dipole interaction to explain the observed efficient excitation transfer from the conjugated polymer to the QD.[54,55] They found Förster radii of 5−7 nm which corresponds to the distance between donor and acceptor where 50% of the excitations are being transferred. The upper value of 7 nm for the Förster radius is considered here for the estimation. On the basis of the morphological study, average values for the outer NW diameter and the PPV shell thickness are 220 and 20 nm, respectively. The estimated proportion of clusters under influence of FRET is about 15% of the total clusters amount. Thus, only a minor proportion of the clusters units could interact with PPV excitons. Dexter energy transfer can also be ruled out in the emission pathways of these hybrid nanowires. The Dexter mechanism is a short-range process involving electron exchange occurring within about 1 nm between donor and acceptor. The main consequence of Dexter transfer is PL quenching. Thus, one should speculate that if this transfer exists in our hybrid nanowires it should affect only the core−shell interface, and thus involve a negligible fraction of clusters at the interface. Similarly, only a very small proportion of clusters would be affected by charge transfers from the PPV shell to the clusters through the insulating PMMA matrix by hopping mechanism. Accordingly, Figure 6 shows that there is no significant PL quenching in the hybrid coaxial nanowires with respect to pure PPV nanotubes or cluster-PMMA NWs.

Beyond the original strategy proposed in this work to minimize the interactions between the luminophores of each color, the coaxial structure can be extended to any couple of luminophores, including the donor−acceptor systems. Then, the proportion of donors located in the shell and acceptors in the core which experiences charge and energy transfers could be tuned by the control of the outer diameter and shell thickness in relation to the characteristic physical lengths involved. For a fixed shell thickness and when RET mechanisms are involved, the relative contribution of donor−acceptor coupling would increase when the diameter is decreased. Thus, the coaxial design could be further exploited to explore the chromaticity diagram, including the white panel by incorporating blue emitters. It is also a promising way to help understanding the complex coupling mechanisms implicated within nanosources made of at least two types of luminophores. This is a central point in this very active field of research, in relation with some of the challenges of nanophotonics, for example by forecasting the emission color of integrated devices.

CONCLUSION

Two-luminophore nanowires based on a coaxial architecture have been designed to take control of the color of hybrid nanosources. The two luminophores, $(n\text{-}Bu_4N)_2[Mo_6Br_8F_6]$ cluster compound and semiconducting PPV conjugated polymer, were selected to restrain the absorption and emission spectral overlapping while a spatial separation was achieved by the coaxial geometry. A wetting template process was used to fabricate the coaxial nanowires with a PPV shell and $(n\text{-}Bu_4N)_2[Mo_6Br_8F_6]$@PMMA core. A systematic study of the micro-PL coupled with micro-Raman investigations along the coaxial nanowires shows that the resulting PL spectra can be simply decomposed by the sum of the spectrum of each luminophore weighted by the relative proportion of each material. A time-resolved PL study confirms that the coupling between the two luminophores can be neglected. The present investigation reveals that it is possible to forecast the color of the emitting coaxial NW on the chromaticity diagram as an interpolation of the CIE coordinates of each luminophore. Additionally, this coaxial morphology offers a promising way to get a sharp change of the color at the nanoscale, as shown here for red, green and yellow emitting segments. This original design is a relevant way to produce hybrid nanosources by in-solution processing with a great versatility in the color control, and thus to address an important challenge of nanophotonics for tagging, sensing, lasing and lighting development.

METHODS

Cluster Synthesis and Composite Preparation. $(n\text{-}Bu_4N)_2[Mo_6Br_8F_6]$ was prepared according to procedure reported.[38] For the fabrication of the $(n\text{-}Bu_4N)_2[Mo_6Br_8F_6]$@PMMA composite, acetone (optical spectroscopy grade, Carlo Erba) and PMMA (M_w: 120 000 g·mol^{-1}, Sigma-Aldrich) were used without further purification. To get an appropriate viscosity for the PMMA and clusters in acetone, a

solution containing 4 wt % of $(n\text{-}Bu_4N)_2[Mo_6Br_8F_6]$ and 10 wt % of PMMA was prepared.

Fabrication of the Coaxial NWs. The coaxial NWs were fabricated by a wetting template method in anodic alumina oxide (AAO) nanoporous template. Commercial AAO membranes purchased from Whatman (anodisc 13) have been used. They are 60 μm thick with a real pore diameter showing a polydispersity between 200 nm and around 250 nm, as revealed by SEM analysis.

For the synthesis of coaxial NWs, two steps of wetting are required. The first step consists in the wetting of AAO membrane with the PPV precursor in methanol solution. The sulfonium polyelectrolyte used as a precursor polymer of PPV was synthesized in our laboratory *via* the standard procedure.[56] To obtain PPV nanotubes, the concentration of PPV precursor in methanol was chosen at 0.5 mg/mL and 200 μL of this solution was drop-casted on AAO membrane, as described elsewhere.[39,47] The precursor embedded in AAO membrane was then thermally converted under a dynamic secondary vacuum ($\sim 10^{-6}$ Torr) for 4 h to obtain PPV. The coaxial nanowires are then obtained by a secondary-template strategy. The AAO membrane containing PPV nanotubes was wetted with the solution containing $TBA^+[Mo_6Br_8F_6]^{2-}$ and PMMA in acetone. The wetted templates were left overnight under ambient condition to allow solvent evaporation. For some characterization, the AAO templates containing coaxial NWs was completely etched in H_3PO_4 (25 wt %) overnight and washed several time with DI water. The coaxial NWs were homogeneously dispersed in DI water solution by ultrasonication during $\sim$10 s with a power of 140 W (Fisher Scientific FB 15052). Ultrasonication results in the shortening of the nanowire length.

Structural and Optical Characterizations. A field-effect scanning electron microscope (JEOL, JSM-7600F operating at 5 kV), an AFM (Nanowizard II, JPK instruments) working in intermittent-contact mode in air with Si tips (PPP-NCHR, Nanosensors) and a transmission electron microscope (Hitachi H9000 NAR operating at 300 kV) were used to investigate the morphology and the composition of the nanowires. For SEM, AFM and fluorescence microscopy experiments, a drop of solution ($\sim$10 μL) containing the nanowires was deposited onto silicon or glass substrates after the dissolution of the template. For TEM experiments (imaging, electron diffraction and EDX), a drop of the solution was deposited on TEM copper grids covered with a thin holey carbon film. The microscope is equipped with a Noran Kevex Si−Li detector for EDX spectroscopy. Epi-fluorescence micrographs were acquired using a calibrated microscope (Eclipse Ti, Nikon) equipped with a $\times$60 objective and a CCD camera, 130 W Hg lamp and fluorescence filter cube (EX 330-380, Dm: 400, BA 420).

Spectroscopic Characterizations. All characterizations were performed at room temperature. Absorption and photoluminescence of the $[Mo_6Br_8F_6]^{2-}$ clusters were measured on spin-coated thin films (1500 rpm, 30 s) deposited on glass from a solution containing 4 wt % in acetone and from a PPV precursor (PPV precursor: 0.5 mg·mL^{-1} in methanol, 1500 rpm, 30 s, thermal conversion at 300 °C for 3 h). UV−vis absorption on thin film sample was performed with a Perkin-Elmer double beam spectrophotometer equipped with an integrating sphere; we carried out PLE measurements using a Jobin-Yvon Fluorolog 3 equipped with a CCD camera and PL experiments on film were achieved under 400 nm excitation at 0.5 mW by a Spectra-Physics Hurricane X laser. For micro-Raman and microphotoluminescence studies, the template containing the nanowires was broken to reveal a cross section and consequently the whole length of the nanowires. Micro-Raman spectra were recorded using a Renishaw in*Via* Raman microscope equipped with a 785 nm line of a HPNIR diode laser. We measured steady-state micro-PL spectra with a Jobin-Yvon T64000 spectrometer under 457.9 nm laser excitation obtained by an argon ion laser. In each case, the spot size of the focused laser beam on the sample was estimated to be about 1−2 μm. The output laser power incident on the sample and the acquisition time were fixed at 5 mW and 90 s, and at 10 μW and 10 s for each Raman and PL spectrum, respectively. Investigation of the effect of the pumping wavelength was performed with Jobin-Yvon T64000 and Horiba Jobin-Yvon iHR 320 spectrometers under 457.9, 488, and 334 nm laser excitation from an argon ion laser. The transient PL experiments have been achieved under 400 nm excitation using Spectra-Physics Hurricane X laser system (82 fs, 1 kHz) onto mat of NWs. The collected emission was temporally detected with a streak camera (Hamamatsu C7700) coupled with an imaging spectrograph. The laser pump power impinging on sample was kept at 0.5 mW to minimize sample photobleaching.

Conflict of Interest: The authors declare no competing financial interest.

Acknowledgment. A. Garreau benefits from a Region Pays de la Loire grant through the Nanofonc network. This work has also been supported by a financial support of the C'Nano Nord-Ouest network. The authors thank J. Y. Mevellec for his help in micro-Raman spectroscopy studies and N. Stephant and S. Grolleau for SEM characterization. We gratefully acknowledge A. Moissette from LASIR Lille I, France, for the PL spectroscopy measurements under UV excitation.

Supporting Information Available: The structure of the $[Mo_6Br^i_8F^a_6]^{2-}$ anionic unit, the description of the method used for the fit of PL spectra, and the photoluminescence excitation maps for thin film of PPV and $(n\text{-}Bu_4N)_2[Mo_6Br_8F_6]$@PMMA are reported. This material is available free of charge *via* the Internet at http://pubs.acs.org.

REFERENCES AND NOTES

1. Li, X.; Wang, T.; Zhang, J.; Zhu, D.; Zhang, X.; Ning, Y.; Zhang, H.; Yang, B. Controlled Fabrication of Fluorescent Barcode Nanorods. *ACS Nano* **2010**, *4*, 4350–4360.
2. Park, D. H.; Hong, Y. K.; Cho, E. H.; Kim, M. S.; Kim, D.-C.; Bang, J.; Kim, J.; Joo, J. Light-Emitting Color Barcode Nanowires Using Polymers: Nanoscale Optical Characteristics. *ACS Nano* **2010**, *4*, 5155–5162.
3. Gu, F.; Zhang, L.; Yin, X.; Tong, L. Polymer Single-Nanowire Optical Sensors. *Nano Lett.* **2008**, *8*, 2757–2761.
4. Zhao, Y. S.; Wu, J.; Huang, J. Vertical Organic Nanowire Arrays: Controlled Synthesis and Chemical Sensors. *J. Am. Chem. Soc.* **2009**, *131*, 3158–3159.
5. Zang, L.; Che, Y.; Moore, J. S. One-Dimensional Self-Assembly of Planar pi-Conjugated Molecules: Adaptable Building Blocks for Organic Nanodevices. *Acc. Chem. Res.* **2008**, *41*, 1596–1608.
6. Che, Y.; Yang, X.; Loser, S.; Zang, L. Expedient Vapor Probing of Organic Amines Using Fluorescent Nanofibers Fabricated from an n-Type Organic Semiconductor. *Nano Lett.* **2008**, *8*, 2219–2223.
7. O'Carroll, D.; Lieberwirth, I.; Redmond, G. Microcavity Effects and Optically Pumped Lasing in Single Conjugated Polymer Nanowires. *Nat. Nanotechnol.* **2007**, *2*, 180–184.
8. Zhao, Y. S.; Peng, A.; Fu, H.; Ma, Y.; Yao, J. Nanowire Waveguides and Ultraviolet Lasers Based on Small Organic Molecules. *Adv. Mater.* **2008**, *20*, 1661–1665.
9. Kuo, C.-C.; Lin, C.-H.; Chen, W.-C. Morphology and Photophysical Properties of Light-Emitting Electrospun Nanofibers Prepared from Poly(fluorene) Derivative/PMMA Blends. *Macromolecules* **2007**, *40*, 6959–6966.
10. Yang, H.; Lightner, C. R.; Dong, L. Light-Emitting Coaxial Nanofibers. *ACS Nano* **2012**, *6*, 622–628.
11. Lu, X.; Zhang, W.; Wang, C.; Wen, T.-C.; Wei, Y. One-Dimensional Conducting Polymer Nanocomposites: Synthesis, Properties and Applications. *Prog. Polym. Sci.* **2011**, *36*, 671–712.
12. Kim, F. S.; Ren, G.; Jenekhe, S. A. One-Dimensional Nanostructures of π-Conjugated Molecular Systems: Assembly, Properties, and Applications from Photovoltaics, Sensors, and Nanophotonics to Nanoelectronics. *Chem. Mater.* **2011**, *23*, 682–732.
13. Long, Y.-Z.; Li, M.-M.; Gu, C.; Wan, M.; Duvail, J.-L.; Liu, Z.; Fan, Z. Recent Advances in Synthesis, Physical Properties and Applications of Conducting Polymer Nanotubes and Nanofibers. *Prog. Polym. Sci.* **2011**, *36*, 1415–1442.
14. Zhao, Y. S.; Fu, H.; Peng, A.; Ma, Y.; Liao, Q.; Yao, J. Construction and Optoelectronic Properties of Organic

One-Dimensional Nanostructures. *Acc. Chem. Res.* **2009**, *43*, 409–418.
15. Dennis, A. M.; Bao, G. Quantum Dot-Fluorescent Protein Pairs as Novel Fluorescence Resonance Energy Transfer Probes. *Nano Lett.* **2008**, *8*, 1439–1445.
16. Stoferle, T.; Scherf, U.; Mahrt, R. F. Energy Transfer in Hybrid Organic/Inorganic Nanocomposites. *Nano Lett.* **2009**, *9*, 453–456.
17. Camposeo, A.; Di Benedetto, F.; Cingolani, R.; Pisignano, D. Full Color Control and White Emission from Conjugated Polymer Nanofibers. *Appl. Phys. Lett.* **2009**, *94*, 043109.
18. Zhao, Y. S.; Fu, H. B.; Hu, F. Q.; Peng, A. D.; Yang, W. S.; Yao, J. N. Tunable Emission from Binary Organic One-Dimensional Nanomaterials: An Alternative Approach to White-Light Emission. *Adv. Mater.* **2008**, *20*, 79–83.
19. Fardy, M.; Yang, P. Materials Science: Lilliputian Light Sticks. *Nature* **2008**, *451*, 408–409.
20. Vohra, V.; Calzaferri, G.; Destri, S.; Pasini, M.; Porzio, W.; Botta, C. Toward White Light Emission through Efficient Two-Step Energy Transfer in Hybrid Nanofibers. *ACS Nano* **2010**, *4*, 1409–1416.
21. Giansante, C.; Raffy, G.; Schafer, C.; Rahma, H.; Kao, M.-T.; Olive, A. G. L.; Del Guerzo, A. White-Light-Emitting Self-Assembled NanoFibers and Their Evidence by Microspectroscopy of Individual Objects. *J. Am. Chem. Soc.* **2011**, *133*, 316–325.
22. Basak, S.; Chandrasekar, R. Multiluminescent Hybrid Organic/Inorganic Nanotubular Structures: One-Pot Fabrication of Tricolor (Blue-Red-Purple) Luminescent Parallelepipedic Organic Superstructure Grafted with Europium Complexes. *Adv. Funct. Mater.* **2011**, *21*, 667–673.
23. Sui, X. M.; Shao, C. L.; Liu, Y. C. White-Light Emission of Polyvinyl Alcohol/ZnO Hybrid Nanofibers Prepared by Electrospinning. *Appl. Phys. Lett.* **2005**, *87*, 113115.
24. Moynihan, S.; Iacopino, D.; O'Carroll, D.; Doyle, H.; Tanner, D. A.; Redmond, G. Emission Colour Tuning in Semiconducting Polymer Nanotubes by Energy Transfer to Organo-Lanthanide Dopants. *Adv. Mater.* **2007**, *19*, 2474–2479.
25. Zhang, H.; Song, H.; Dong, B.; Han, L.; Pan, G.; Bai, X.; Fan, L.; Lu, S.; Zhao, H.; Wang, F. Electrospinning Preparation and Luminescence Properties of Europium Complex/Polymer Composite Fibers. *J. Phys. Chem. C* **2008**, *112*, 9155–9162.
26. Bredas, J.-L.; Beljonne, D.; Coropceanu, V.; Cornil, J. Charge-Transfer and Energy-Transfer Processes in pi-Conjugated Oligomers and Polymers: A Molecular Picture. *Chem. Rev.* **2004**, *104*, 4971–5003.
27. McGehee, M. D.; Bergstedt, T.; Zhang, C.; Saab, A. P.; O'Regan, M. B.; Bazan, G. C.; Srdanov, V. I.; Heeger, A. J. Narrow Bandwidth Luminescence from Blends with Energy Transfer from Semiconducting Conjugated Polymers to Europium Complexes. *Adv. Mater.* **1999**, *11*, 1349–1354.
28. Forster, T. Transfer Mechanisms of Electronic Excitation. *Discuss. Faraday Soc.* **1959**, *27*, 7–17.
29. Halivni, S.; Sitt, A.; Hadar, I.; Banin, U. Effect of Nanoparticle Dimensionality on Fluorescence Resonance Energy Transfer in Nanoparticle-Dye Conjugated Systems. *ACS Nano* **2012**, *6*, 2758–2765.
30. Dexter, D. L. A Theory of Sensitized Luminescence in Solids. *J. Chem. Phys.* **1953**, *21*, 836–850.
31. Scholes, G. D.; Rumbles, G. Excitons in Nanoscale Systems. *Nat. Mater.* **2006**, *5*, 683–696.
32. Kamtekar, K. T.; Monkman, A. P.; Bryce, M. R. Recent Advances in White Organic Light-Emitting Materials and Devices (WOLEDs). *Adv. Mater.* **2010**, *22*, 572–582.
33. Gather, M. C.; Köhnen, A.; Meerholz, K. White Organic Light-Emitting Diodes. *Adv. Mater.* **2011**, *23*, 233–248.
34. Simbrunner, C.; Hernandez-Sosa, G.; Quochi, F.; Schwabegger, G. N.; Botta, C.; Oehzelt, M.; Salzmann, I.; Djuric, T.; Neuhold, A.; Resel, R.; et al. Color Tuning of Nanofibers by Periodic Organic-Organic Hetero-Epitaxy. *ACS Nano* **2012**, *6*, 4629–4638.
35. Molard, Y.; Dorson, F.; Cîrcu, V.; Roisnel, T.; Artzner, F.; Cordier, S. Clustomesogens: Liquid Crystal Materials Containing Transition-Metal Clusters. *Angew. Chem., Int. Ed.* **2010**, *49*, 3351–3355.
36. Mocanu, A. S.; Amela-Cortes, M.; Molard, Y.; Circu, V.; Cordier, S. Liquid Crystal Properties Resulting from Synergetic Effects between Non-Mesogenic Organic Molecules and a One Nanometre Sized Octahedral Transition Metal Cluster. *Chem. Commun.* **2011**, *47*, 2056–2058.
37. Molard, Y.; Ledneva, A.; Amela-Cortes, M.; Cîrcu, V.; Naumov, N. G.; Mériadec, C.; Artzner, F.; Cordier, S. Ionically Self-Assembled Clustomesogen with Switchable Magnetic/Luminescence Properties Containing $[Re_6Se_8(CN)_6]n-$ (n = 3, 4) Anionic Clusters. *Chem. Mater.* **2011**, *23*, 5122–5130.
38. Dybtsev, D.; Serre, C.; Schmitz, B.; Panella, B.; Hirscher, M.; Latroche, M.; Llewellyn, P. L.; Cordier, S.; Molard, Y.; Haouas, M.; et al. Influence of $[Mo_6Br_8F_6]^{2-}$ Cluster Unit Inclusion within the Mesoporous Solid MIL-101 on Hydrogen Storage Performance. *Langmuir* **2010**, *26*, 11283–11290.
39. Lorcy, J. M.; Massuyeau, F.; Moreau, P.; Chauvet, O.; Faulques, E.; Wery, J.; Duvail, J. L. Coaxial Nickel/Poly(p-phenylene vinylene) Nanowires as Luminescent Building Blocks Manipulated Magnetically. *Nanotechnology* **2009**, *20*, 405601.
40. Bublitz, D.; Preetz, W. Schwingungsspektren und Normalkoordinatenanalysen der ^{92}Mo-, ^{100}Mo-, ^{35}Cl- und ^{37}Cl-Isotopomeren der Clusteranionen $[(Mo_6X^i_8)Y^a_6]^{2-}$; X^i = Cl, Br; Y^a = F, Cl, Br, I. *Z. Anorg. Allg. Chem.* **1996**, *622*, 1107–1117.
41. Ramirez-Tagle, R.; Arratia-Pérez, R. Electronic Structure and Molecular Properties of the $[Mo_6X_8L_6]^{2-}$; X = Cl, Br, I; L = F, Cl, Br, I Clusters. *Chem. Phys. Lett.* **2008**, *460*, 438–441.
42. Schoonover, J. R.; Zietlow, T. C.; Clark, D. L.; Heppert, J. A.; Chisholm, M. H.; Gray, H. B.; Sattelberger, A. P.; Woodruff, W. H. Resonance Raman Spectra of $[M_6X_8Y_6]^{2-}$ Cluster Complexes (M = Mo, W; X, Y = Cl, Br, I). *Inorg. Chem.* **1996**, *35*, 6606–6613.
43. Willis, H. A.; Zichy, V. J. I.; Hendra, P. J. The Laser-Raman and Infra-Red Spectra of Poly(methyl methacrylate). *Polymer* **1969**, *10*, 737–746.
44. Xu, X.; Ming, H.; Zhang, Q.; Zhang, Y. Properties of Raman Spectra and Laser-Induced Birefringence in Polymethyl Methacrylate Optical Fibres. *J. Opt. A: Pure Appl. Opt.* **2002**, *4*, 237.
45. Thomas, K. J.; Sheeba, M.; Nampoori, V. P. N.; Vallabhan, C. P. G.; Radhakrishnan, P. Raman Spectra of Polymethyl Methacrylate Optical Fibres Excited by a 532 nm Diode Pumped Solid State Laser. *J. Opt. A: Pure Appl. Opt.* **2008**, *10*, 055303.
46. Mulazzi, E.; Perego, R.; Aarab, H.; Mihut, L.; Lefrant, S.; Faulques, E.; Wery, J. Photoconductivity and Optical Properties in Composites of Poly(paraphenylene vinylene) and Single-Walled Carbon Nanotubes. *Phys. Rev. B* **2004**, *70*, 155206.
47. Massuyeau, F.; Duvail, J. L.; Athalin, H.; Lorcy, J. M.; Lefrant, S.; Wery, J.; Faulques, E. Elaboration of Conjugated Polymer Nanowires and Nanotubes for Tunable Photoluminescence Properties. *Nanotechnology* **2009**, *20*, 155701.
48. Maverick, A. W.; Najdzionek, J. S.; MacKenzie, D.; Nocera, D. G.; Gray, H. B. Spectroscopic, Electrochemical, and Photochemical Properties of Molybdenum(II) and Tungsten(II) Halide Clusters. *J. Am. Chem. Soc.* **1983**, *105*, 1878–1882.
49. Szczepura, L.; Edwards, J.; Cedeño, D. Luminescent Properties of Hexanuclear Molybdenum(II) Chloride Clusters Containing Thiolate Ligands. *J. Cluster Sci.* **2009**, *20*, 105–112.
50. Mulazzi, E.; Ripamonti, A.; Wery, J.; Dulieu, B.; Lefrant, S. Theoretical and Experimental Investigation of Absorption and Raman Spectra of Poly(paraphenylene vinylene). *Phys. Rev. B* **1999**, *60*, 16519–16525.
51. Stubinger, T.; Brutting, W. Exciton Diffusion and Optical Interference in Organic Donor-Acceptor Photovoltaic Cells. *J. Appl. Phys.* **2001**, *90*, 3632–3641.
52. Markov, D. E.; Amsterdam, E.; Blom, P. W. M.; Sieval, A. B.; Hummelen, J. C. Accurate Measurement of the Exciton Diffusion Length in a Conjugated Polymer Using a Heterostructure with a Side-Chain Cross-Linked Fullerene Layer. *J. Phys. Chem. A* **2005**, *109*, 5266–5274.
53. Lakowicz, J. R. *Principles of Fluorescence Spectroscopy*, 3rd ed.; Springer: New York, 2006.

54. Anni, M.; Manna, L.; Cingolani, R.; Valerini, D.; Creti, A.; Lomascolo, M. Forster Energy Transfer from Blue-Emitting Polymers to Colloidal CdSe/ZnS Core Shell Quantum Dots. *Appl. Phys. Lett.* **2004**, *85*, 4169–4171.
55. Kaufmann, S.; Stoferle, T.; Moll, N.; Mahrt, R. F.; Scherf, U.; Tsami, A.; Talapin, D. V.; Murray, C. B. Resonant Energy Transfer Within a Colloidal Nanocrystal Polymer Host System. *Appl. Phys. Lett.* **2007**, *90*, 071108.
56. Stenger-Smith, J. D.; Lenz, R. W.; Wegner, G. Spectroscopic and Cyclic Voltammetric Studies of Poly(p-phenylene vinylene) Prepared from Two Different Sulphonium Salt Precursor Polymers. *Polymer* **1989**, *30*, 1048–1053.